MOEM

Modern Electronic Materials 2023; 9(4): 163–168
DOI 10.3897/j.moem.9.4.115181

Research Article

Synthesis and piezoelectric properties of freestanding ferroelectric films based on barium strontium titanate

Mikhail S. Afanasiev[1], Dmitry A. Kiselev[1,2], Alexey A. Sivov[1], Galina V. Chucheva[1]

1 *Kotelnikov Institute of Radio Engineering and Electronics of the Russian Academy of Sciences (Fryazino Branch), 1 Vvedenskogo Sq., Fryazino, Moscow Region 141120, Russian Federation*

2 *National University of Science and Technology "MISIS", 4-1 Leninsky Ave., Moscow 119049, Russian Federation*

Corresponding author: Dmitry A. Kiselev (dm.kiselev@gmail.com)

Received 9 November 2023 ♦ **Accepted** 26 November 2023 ♦ **Published** 12 December 2023

Citation: Afanasiev MS, Kiselev DA, Sivov AN, Chucheva GV (2023) Synthesis and piezoelectric properties of freestanding ferroelectric films based on barium strontium titanate. *Modern Electronic Materials* 9(4): 163–168. https://doi.org/10.3897/j.moem.9.4.115181

Abstract

In this work, the membrane structures based on lead-free ferroelectric barium strontium titanate with composition $Ba_{0.8}Sr_{0.2}TO_3$ (BSTO) were fabricated by a magnetron sputtering method. The formation of a single-phase $Ba_{0.8}Sr_{0.2}TO_3$ with thickness of 300 nm sintered on Si substrate is confirmed by XRD analysis. It is shown that films without a silicon substrate exhibit ferroelectric and piezoelectric properties. The piezoelectric and ferroelectric behaviors of BSTO thin film without a silicon substrate were confirmed through a piezoelectric force microscopy and Kelvin probe force microscopy and measurements of the effective piezoelectric coefficients (d_{33} and d_{15}). Images of the residual potential of polarized areas have been obtained on the membranes, which are stable over time despite the absence of a lower electrode. Additionally, a local of ferroelectric hysteresis loop has been observed. A combination of the structural and piezoelectric measurements reveals that it possible to create freestanding ferroelectric films based on $Ba_{0.8}Sr_{0.2}TO_3$ system, establishing it as a promising candidate for high-performance electromechanical applications.

Keywords

ferroelectric domain structure, ferroelectric membrane, hysteresis, piezoelectric properties, structure

1. Introduction

Electromechanical energy conversion of piezoelectric materials is the basis for a wide range of sensor and communication technologies, including those used for ultrasound imaging and cell phones [1–3]. For electromechanical energy harvesting [4, 5], as well as flexible electronics [6, 7], nanomotors [8] and medical applications [9–11], it is necessary to obtain flexible piezoelectric materials and create devices based on these materials. Modern areas of piezoelectric applications include thin-film technologies [12–14]; however, the film substrates are usually rigid, which hinders the development of flexible devices. Therefore, flexible piezoelectric devices are typically based on either nanowires [4] or thin film systems, but with substrates that have been developed specially for such applications [15, 16]. Most piezoelectrics that have found practical application are lead based on oxide materials with high piezoelectric coefficients. However, the toxicity of these materials is undesirable for environmental reasons and makes them unsuitable for medical use. In addition, the traditional thin-film geometry limits electromechanical excitation modes. That is, a uniaxial electric field leads, as a rule, to parallel or perpendicular

uniaxial or biaxial mechanical deformation (or vice versa). However, interest in flexible electronic technologies is generating a new need for improved electromechanical excitation modes [17]. Removing the substrate for piezoelectric films or membranes increases their functional properties [18–21] mainly due to mechanically induced reorganization of ferroelectric domains [22]. However, the production of films without a substrate remains a challenge.

Lu et al. [23] recently demonstrated a general method for preparing oxide materials in the form of membranes, i.e., continuous free-standing thin films without substrates. Dong et al. [24], have used this method to treat $BaTiO_3$ membranes, which are a well-known lead-free piezoelectric and ferroelectric material. Superelasticity and superflexibility, which arise from the irregular dynamics of ferroelectric domains in these membranes, have been demonstrated. Folded membranes based on $BaTiO_3$ (BTO)/poly(dimethylsiloxane) with finely controlled parallel, zigzag and mosaic patterns were also prepared [25]. Self-assembled membranes with periodic folded patterns are critical building blocks of various flexible electronics, where folds are typically designed and fabricated to provide various functionalities. These membranes are typically metallic and organic materials with good ductility that are resistant to complex deformations. However, the production of membranes based on oxide materials is challenging due to their inherent strong covalent or ionic bonding, which usually leads to cracking and destruction. BTO layers exhibit excellent flexibility and can form well-ordered and periodic folds when compressed in the stress plane. Increased piezoelectricity is observed in the areas of peaks and valleys, where the largest strain gradient is generated. Atomistic simulations also showed that elasticity and the correlated interaction between polarization and strain-strain gradient are closely related to ferroelectric domain switching and continuous dipole rotation. Out-of-plane polarization is mainly generated in compression regions, while in-plane polarization dominates in tension regions. Wrinkled ferroelectric oxides with different strain regions and correlated polarization distributions would pave the way for new flexible electronics.

Another key component of a dynamic, large-area, deformable, and wearable sensing device is the creation of flexible thin-film electrodes. An ideal flexible conductive material should have high electrical conductivity and strength even under extreme and complicated mechanical deformation conditions. In addition, mechanical flexibility and stability are priority characteristics for research and development.

2. Objects and research methods

For our study, a silicon membrane with a ferroelectric film of BSTO composition deposited on its surface was prepared as shown in Fig. 1 *a*. The silicon membrane was formed by using a [100] silicon (*p*-type) substrate by liquid photolithography. The diameter of the manufactured silicon membranes at the base was ~1.2 mm and the membrane thickness was 20 μm (see Fig. 1 *b*).

The BSTO film deposition was carried out by high-frequency **(RF)** sputtering of a stoichiometric target of the same composition at elevated oxygen pressures on a Plasma 50 SE installation. Sputtering of the BSTO films was performed under the following conditions: oxygen pressure during the sputtering process was 60 Pa; the distance between target and substrate was 10 mm; the substrate temperature was 630 °C. The film growth rate was ~6.0 nm/min at these conditions. The crystal structure of BSTO films was studied by X-ray diffraction analysis on an automated double-crystal diffractometer DRON-3 operating according to the Bragg–Brentano scheme. An X-ray tube with a copper anode was used as a radiation source with the wavelength of 0.1541 nm. A quartz monochromator was used to isolate the $K_{\alpha 1}$ line from the spectrum.

To visualize the surface, piezoelectric response and surface potential signal, a scanning probe microscope Ntegra Prima (NT-MDT Spectrum Instruments, Russia) was used. The measurements were carried out by using the piezoelectric response force microscopy (the MCos signal was recorded) by applying an alternating voltage with an amplitude of 3 V and a frequency of 27 kHz to a conducting probe, as well as in the Kelvin mode using

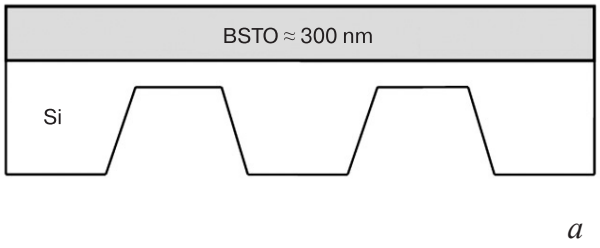

a

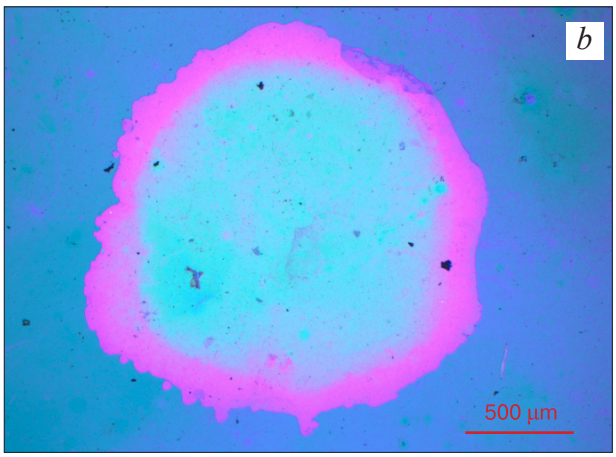

Figure 1. Schematic representation of the fabricated structure (*a*); optical image of the membrane (top view) (*b*)

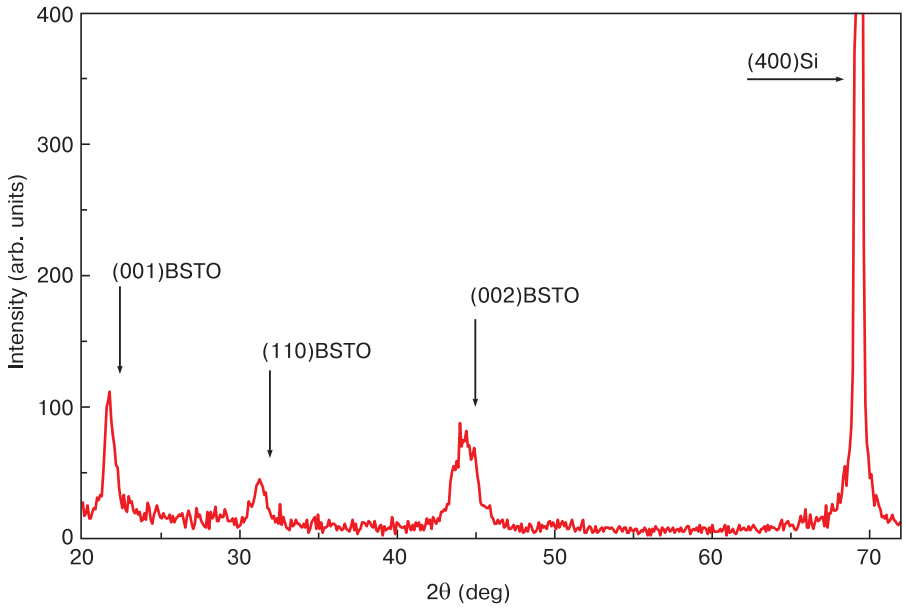

Figure 2. X-ray diffraction pattern of BSTO film

probes of the NSG10/Pt series to record the surface potential signal. The scanning area did not exceed 20 × 20 μm^2.

3. Results and discussion

The results of X-ray diffraction analysis of the BSTO film are shown in Fig. 2. The diffraction pattern clearly shows lines corresponding to the (001) and (110) BSTO planes. Based on the intensity ratio of the (001)/(110) BSTO peaks, one can state that the predominant orientation is (001). Also, the film reflexes are shifted toward smaller angles. This means that the lattice parameters shifted upward with respect to the table ones by approximately 0.5%, which indicates a small deviation between the film compositions. The average size of the coherent scattering regions estimated from the width of the X-ray peaks was about 5 nm.

The BSTO membrane surface, visualized using a scanning probe microscope, has a grain structure with an average crystallite size of 150–200 nm and roughness parameters: Rz = 5.1 nm and Ra = 4.0 nm (Fig. 3 *a*). Contrast areas that have a certain direction of polarization are visible on the vertical (Fig. 3 *b*) and lateral (Fig. 3 *c*) piezoresponse signals.

To calculate the values of the effective piezoelectric coefficients d_{33} and d_{15}, we have used the methodology proposed in the work [26].

An alternating voltage of varying amplitude (from 1 to 10 V) with a frequency of 27 kHz, which is much lower than the contact resonance frequency of the probe-sample system, was applied to the cantilever of a scanning probe microscope, and the deformation of the sample under the influence of alternating voltage was recorded in units of picometers. Next, the values of d_{33} (based on the vertical piezoresponse signal) and d_{15} (based on the lateral piezoresponse signal) were found from the approximation by a linear function of the resulting deformations. The results of calculations are presented in Fig. 4.

The following numerical values of the effective piezoelectric coefficients on the membrane: d_{33} = 3.1 pm/V and d_{15} = 25.3 pm/V were obtained. In comparison, the values obtained for the BSTO film were d_{33} = 15 pm/V (Fig. 5).

In the process of polarizing the membrane with a constant voltage, it was possible to form stable regions with

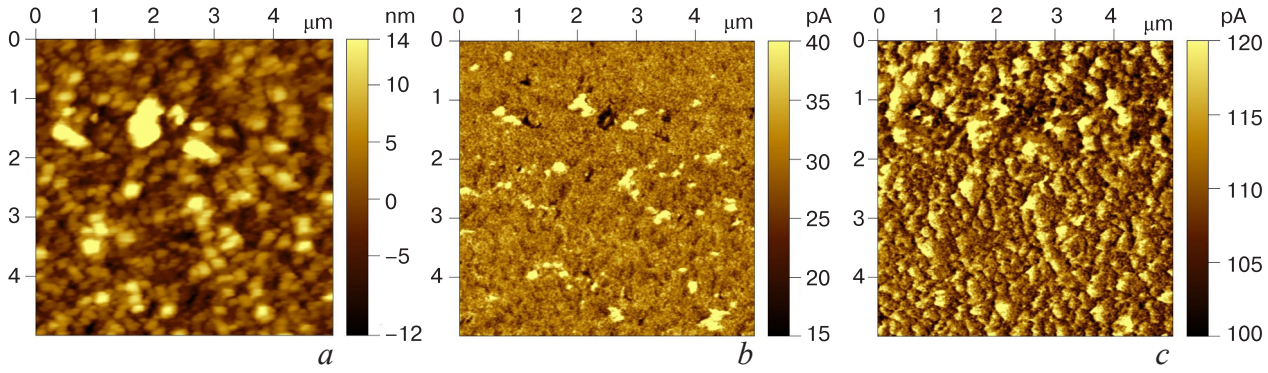

Figure 3. Images of the surface (*a*) of a membrane based on BSTO; vertical piezoresponse signal (*b*); lateral piezoresponse signal (*c*)

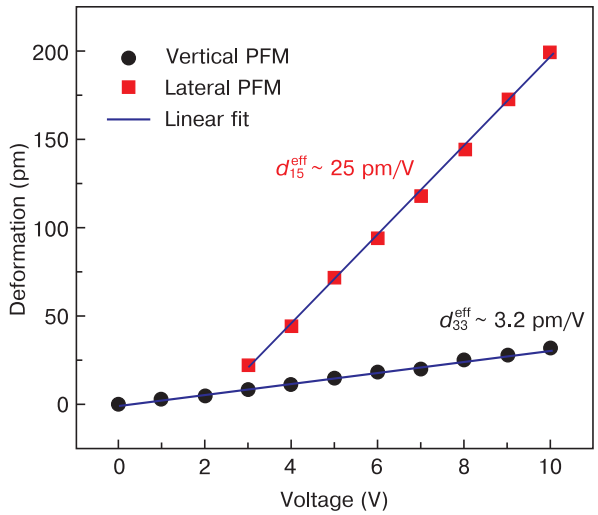

Figure 4. Results of calculations on the effective d_{33} and d_{15} values for a BSTO-based membrane

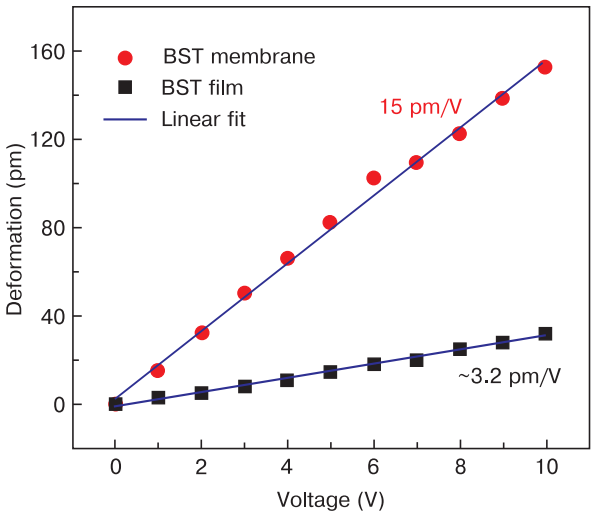

Figure 5. Results of calculations on the effective d_{33} values for a membrane and a film based on BSTO

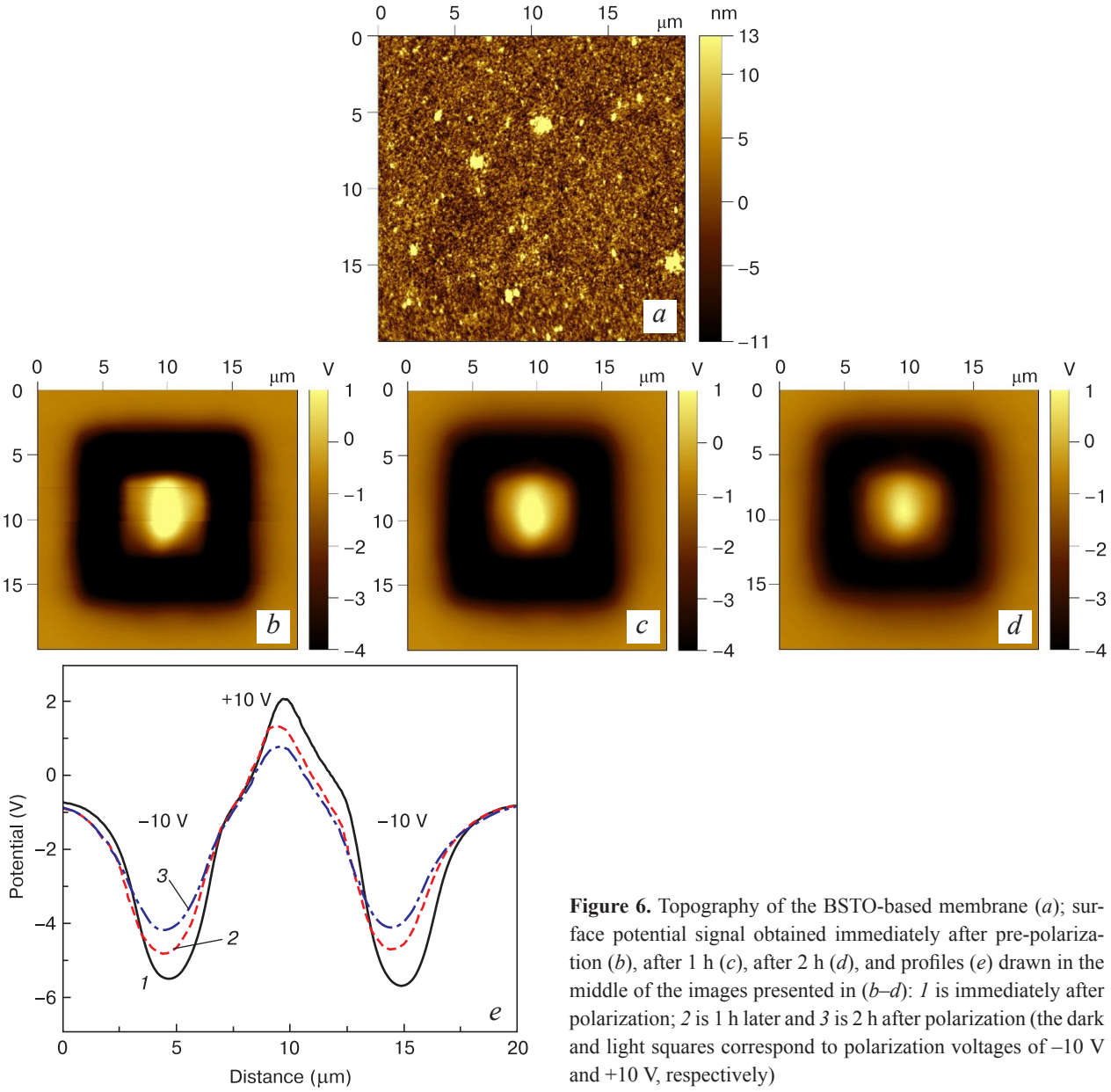

Figure 6. Topography of the BSTO-based membrane (*a*); surface potential signal obtained immediately after pre-polarization (*b*), after 1 h (*c*), after 2 h (*d*), and profiles (*e*) drawn in the middle of the images presented in (*b–d*): *1* is immediately after polarization; *2* is 1 h later and *3* is 2 h after polarization (the dark and light squares correspond to polarization voltages of –10 V and +10 V, respectively)

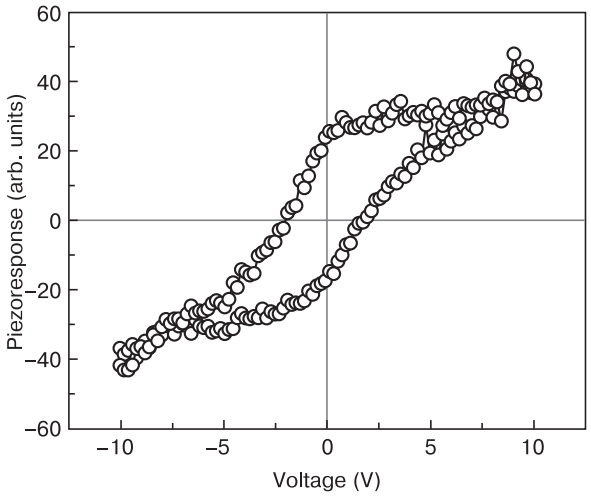

Figure 7. Piezoelectric hysteresis loop of the BSTO membrane

different orientations of polarization from and towards the surface (Fig. 6). It was shown that polarization with a constant voltage does not produce any effect on the membrane surface (Fig. 6 *a*). In the Kelvin mode, the temporal stability of polarized regions, which were preliminarily obtained in the piezoelectric response force microscopy mode, was studied.

In Figs 6 *b*–6 *d*, the "light" square reflects the result of applying a voltage of +10 V to the cantilever of a scanning probe microscope and the "dark" square corresponds to polarization at – 10 V. As was shown earlier [27], the use of the Kelvin mode, which is non-contact, significantly reduces the effects of depolarization of the induced region during scanning compared to the use of the contact scanning mode, where the piezoresponse signal is recorded by applying an alternating voltage comparable to the switching voltage in the case of films less than 100 nm thick.

The analysis showed that the contrast of induced areas, visualized in the Kelvin mode, is well visualized for an extended time. In 2 h after polarization, the signal amplitude of the polarized areas decreased by less than 40% compared to the initial signal obtained immediately after polarization (Fig. 6 *e*).

A local piezoelectric hysteresis loop was obtained, which confirmed the polarization switching and the ferroelectric nature of the BSTO membrane (Fig. 7). The hysteresis loop is characterized by low switching voltage values of ~ 2 V.

4. Conclusion

We have fabricated a structure consisting of a silicon membrane (20 μm thickness) with a deposited BSTO ferroelectric film of 300 nm thickness. The crystal structure and piezoelectric properties of the freestanding BSTO film have been investigated. In the piezoelectric response force microscopy mode, the domain structure of the BSTO film is visualized, the values of effective piezoelectric coefficients and local hysteresis loops are obtained. As a result of the experiment the values d_{33} = 3.1 pm/V and d_{15} = 25.3 pm/V were obtained. Polarized regions after applied a DC voltage of magnitude ±10 V to the cantilever of the scanning probe microscope are stable over time. The presence of a piezoelectric hysteresis loop also confirms the ferroelectric nature of BSTO-based membrane structures.

Acknowledgements

The study was carried out at the expense of grant No. 22-19-00493 of the Russian Science Foundation, https://rscf.ru/project/22-19-00493/.

References

1. Lang C., Fang J., Shao H., Ding X., Lin T. High-sensitivity acoustic sensors from nanofiber webs. *Nature Communications*. 2016; 7(1): 11108. https://doi.org/10.1038/ncomms11108
2. Yang J., Li Z., Xin X., Gao X., Yuan X., Wang Z., Yu Z., Wang X., Zhou J., Dong S. Designing electromechanical metamaterial with full nonzero piezoelectric coefficients. *Science Advances*. 2019; 5(11): eaax1782. https://doi.org/10.1126/sciadv.aax1782
3. Song K., Zhao R., Wang Z.L., Yang Y. Conjuncted pyro-piezoelectric effect for self-powered simultaneous temperature and pressure sensing. *Advanced Materials*. 2019; 31(36): 1902831. https://doi.org/10.1002/adma.201902831
4. Wang Z.L., Song J. Piezoelectric Nanogenerators based on zinc oxide nanowire *Arrays. Science*. 2006; 312(5771): 242–246. https://doi.org/10.1126/science.1124005
5. Qi Y., Kim J., Nguyen T.D., Lisko B., Purohit P.K., McAlpine M.C. Enhanced piezoelectricity and stretchability in energy harvesting devices fabricated from buckled PZT ribbons. *Nano Letters*. 2011; 11(3): 1331–1336. https://doi.org/10.1021/nl104412b
6. Lee J., Lee K.Y., Gupta M.K., Kim T.Y., Lee D., Oh J., Ryu C., Yoo W.J., Kang C., Yoon S., Yoo J., Kim S. Highly stretchable piezoelectric-pyroelectric hybrid nanogenerator. *Advanced Materials*. 2014; 26(5): 765–769. https://doi.org/10.1002/adma.201303570
7. Lee M., Chen C., Wang S., Cha S.N., Park Y.J., Kim J.M., Chou L., Wang Z.L. A hybrid piezoelectric structure for wearable nanogenerators. *Advanced Materials*. 2012; 24(13): 1759–1764. https://doi.org/10.1002/adma.201200150
8. Smith G.L., Pulskamp J.S., Sanchez L.M., Potrepka D.M., Proie R.M., Ivanov T.G., Rudy R.Q., Nothwang W.D., Bedair S.S.,

Meyer C.D., Polcawich R.G. PZT-based piezoelectric MEMS technology. *Journal of the American Ceramic Society*. 2012; 95(6): 1777–1792. https://doi.org/10.1111/j.1551-2916.2012.05155.x

9. Wu N., Cheng X., Zhong Q., Zhong J., Li W., Wang B., Hu B., Zhou J. Cellular polypropylene piezoelectret for human body energy harvesting and health monitoring. *Advanced Functional Materials*. 2015; 25(30): 4788–4794. https://doi.org/10.1002/adfm.201501695
10. Chorsi M.T., Curry E.J., Chorsi H.T., Das R., Baroody J., Purohit P.K., Ilies H., Nguyen T.D. Piezoelectric biomaterials for sensors and actuators. *Advanced Materials*. 2019; 31(1): 1802084. https://doi.org/10.1002/adma.201802084
11. Dagdeviren C., Su Y., Joe P., Yona R., Liu Y., Kim Y.-S., Huang Y., Damadoran A.R., Xia J., Martin L.W., Huang Y., Rogers J.A. Conformable amplified lead zirconate titanate sensors with enhanced piezoelectric response for cutaneous pressure monitoring. *Nature Communications*. 2014; 5(1): 4496. https://doi.org/10.1038/ncomms5496
12. Wang X., He X., Zhu H., Sun L., Fu W., Wang X., Hoong L.C., Wang H., Zeng Q., Zhao W., Wei J., Jin Z., Shen Z., Liu J., Zhang T., Liu Z. Subatomic deformation driven by vertical piezoelectricity from CdS ultrathin films. *Science Advances*. 2016; 2(7): e1600209. https://doi.org/10.1126/sciadv.1600209
13. Saremi S., Xu R., Dedon L.R., Gao R., Ghosh A., Dasgupta A., Martin L.W. Electronic transport and ferroelectric switching in ion-bombarded, defect-engineered $BiFeO_3$ thin films. *Advanced Materials Interfaces.* 2018; 5(3): 1700991. https://doi.org/10.1002/admi.201700991
14. Dedon L.R., Saremi S., Chen Z., Damodaran A.R., Apgar B.A., Gao R., Martin L.W. Nonstoichiometry, structure, and properties of $BiFeO_3$ films. *Chemistry of Materials*. 2016; 28(16): 5952–5961. https://doi.org/10.1021/acs.chemmater.6b02542
15. Tsai M.-F., Jiang J., Shao P.-W., Lai Y.-H., Chen J.-W., Ho S.-Z., Chen Y.-C., Tsai D.-P., Chu Y.-H. Oxide heteroepitaxy-based flexible ferroelectric transistor. *ACS Applied Materials & Interfaces*. 2019; 11(29): 25882–25890. https://doi.org/10.1021/acsami.9b06332
16. Onn Winestook R., Saguy C., Ma C., Chu Y., Ivry Y. Enhanced ferroelectric functionality in flexible lead zirconate titanate films with in situ substrate-clamping compensation. *Advanced Electronic Materials.* 2019; 5(10): 1900428. https://doi.org/10.1002/aelm.201900428
17. Jafferis N.T., Helbling E.F., Karpelson M., Wood R.J. Untethered flight of an insect-sized flapping-wing microscale aerial vehicle. *Nature*. 2019; 570(7762): 491–495. https://doi.org/10.1038/s41586-019-1322-0
18. Choi K.J., Biegalski M., Li Y.L., Sharan A., Schubert J., Uecker R., Reiche P., Chen Y.B., Pan X.Q., Gopalan V., Chen L.-Q., Schlom D.G., Eom C.B. Enhancement of ferroelectricity in strained $BaTiO_3$ thin films. *Science*. 2004; 306(5698): 1005–1009. https://doi.org/10.1126/science.1103218
19. Haeni J.H., Irvin P., Chang W., Uecker R., Reiche P, Li Y.L., Choudhury S., Tian W., Hawley M.E., Craigo B., Tagantsev A.K., Pan X.Q., Streiffer S.K., Chen L.Q., Kirchoefer S.W., Levy J, Schlom D.G. Room-temperature ferroelectricity in strained $SrTiO_3$. *Nature*. 2004; 430(7001): 758–761. https://doi.org/10.1038/nature02773
20. Nagarajan V., Roytburd A., Stanishevsky A., Prasertchoung S., Zhao T., Chen L., Melngailis J., Auciello O., Ramesh R. Dynamics of ferroelastic domains in ferroelectric thin films. *Nature Materials*. 2003; 2(1): 43–47. https://doi.org/10.1038/nmat800
21. Yadav A.K., Nelson C.T., Hsu S.L., Hong Z., Clarkson J.D., Schlepütz C.M., Damodaran A.R., Shafer P., Arenholz E., Dedon L.R., Chen D., Vishwanath A., Minor A.M., Chen L.Q., Scott J.F., Martin L.W., Ramesh R. Observation of polar vortices in oxide superlattices. *Nature.* 2016; 530(7589): 198–201. https://doi.org/10.1038/nature16463
22. Ivry Y., Lyahovitskaya V., Zon I., Lubomirsky I., Wachtel E., Roytburd A.L. Enhanced pyroelectric effect in self-supported films of $BaTiO_3$ with polycrystalline macrodomains. *Applied Physics Letters*. 2007; 90(17): 172905. https://doi.org/10.1063/1.2730749
23. Lu D., Baek D.J., Hong S.S., Kourkoutis L.F., Hikita Y., Hwang H.Y. Synthesis of freestanding single-crystal perovskite films and heterostructures by etching of sacrificial water-soluble layers. *Nature Materials* 2016; 15(12): 1255–1260. https://doi.org/10.1038/nmat4749
24. Dong G., Li S., Yao M., Zhou Z., Zhang Y.-Q., Han X., Luo Z., Yao J., Peng B., Hu Z., Huang H., Jia T., Li J., Ren W., Ye Z.-G., Ding X., Sun J., Nan C.-W., Chen L-Q., Li J., Liu M. Super-elastic ferroelectric single-crystal membrane with continuous electric dipole rotation. *Science*. 2019; 366(6464): 475–479. https://doi.org/10.1126/science.aay7221
25. Dong G., Li S., Li T., Wu H., Nan T., Wang X., Liu H., Cheng Y., Zhou Y., Qu W., Zhao Y., Peng B., Wang Z., Hu Z., Luo Z., Ren W., Pennycook S.J., Li J., Sun J., Ye Z., Jiang Z., Zhou Z., Ding X., Min T., Liu M. Periodic wrinkle-patterned single-crystalline ferroelectric oxide membranes with enhanced piezoelectricity. *Advanced Materials*. 2020; 32(50): 2004477. https://doi.org/10.1002/adma.202004477
26. Yang X., Sun J., Chen G., Yu H., Zhang X., Tang G., Zhou W., Yang Y., Ma C., Hong J., Yang B. Enhancing piezoelectric response in (002)-oriented $Ta_xAl_{(1-x)}N$ films by magnetron-sputtering composition-tunable AlTa alloys. *Journal of the European Ceramic Society*. 2023; 43(14): 6050–6058. https://doi.org/10.1016/j.jeurceramsoc.2023.06.050
27. Zhukov R.N., Bykov A.S., Kiselev D.A., Malinkovich M.D., Parkhomenko Y.N. Piezoelectric properties and surface potential behavior in $LiNbO_3$ thin films grown by the radio frequency magnetron sputtering. *Journal of Alloys and Compounds*. 2014; 586: S336–S338. https://doi.org/10.1016/j.jallcom.2013.01.116